Journal of King Saud University – Computer and Information Sciences 34 (2022) 86–94

Contents lists available at ScienceDirect

Journal of King Saud University – Computer and Information Sciences

journal homepage: www.sciencedirect.com

Microc alcification Segmentation Using Modified U-net Segmentation Network from Mammogram Images

Md Shamim Hossain

School of Science, Edith Cowan University, 6027, Australia

ARTICLE INFO

Article history:
Received 2 June 2019
Revised 30 September 2019
Accepted 30 October 2019
Available online 4 November 2019

Keywords:
Breast mammogram
Fuzzy C-means clustering
Micro-calcification
Modified U-net
Segmentation

ABSTRACT

Breast cancer is the most common aggressive cancer in women while the early detection of this cancer can reduce the aggressiveness. But it is challenging to identify breast cancer features such as micro-calcification from mammogram images by the human eye because of its size and appearance. Therefore, the automatic detection of micro-calcification is essential for diagnosis and proper treatment. This work introduces an automated approach and segments any micro-calcification in the mammogram images. At first, the preprocessing applications of images are applied to enhance the image. After that, the breast region is segmented from the pectoral region. The suspicious regions are detected using fuzzy C-means clustering algorithm and divided them into negative and positive patches. This procedure eliminates the manual labelling of the region of interest. The positive patches which contain micro-calcification pixels are taken to train a modified U-net segmentation network. Finally, the trained network is utilised to segment the micro-calcification area automatically from the mammogram images. This process can help as an assistant to the radiologist for early diagnosis and increase the segmentation accuracy of the micro-calcification regions. The proposed system is trained up with a Digital Database for Screening Mammography (DDSM), which is prepared by the University of South Florida, USA. We obtain 98.5% F-measure and 97.8% Dice score respectively. Besides, Jaccard index is 97.4%. The average accuracy of the proposed method is 98.2% which provides better performance than state-of-the-art methods. This work can be embedded with the real-time mammography system.

1. Introduction

Breast cancer is increasing rapidly in both developing and developed countries. This cancer is the second significant reason of deaths for women in the world. According to the study, 1of 12 women suffers from breast cancer that is why this research seeks to find micro-calcification regions within the mammography images using the pixels of the images to process them through a deep learning U-net segmentation network. The World Health Organization reported that around 508,000 women deaths are directly related to breast cancer (Kaur et al., 2019). However, the highest acceptable diagnosis method of breast cancer analysis is mammography imaging. It is possible to detect the 85% to 90% breast cancer at least two years before by the mammogram screening (Shi et al., 2018). Therefore, mammogram screening is required every two years from the age of 40, which is suggested by the World Health Organization and American Cancer Society to control breast cancer (Pardamean et al., 2018). There are lots of imaging technique to visualise the internal structure of the breast, where mammographic imaging is the best technique. Mammography is an imaging technique like X-ray, and this technique is used to detect breast cancer so that women can be treated with the appropriate treatments. The visual information of mammogram provides tissues and microstructure of the breast regions (Li et al., 2019). The dense tissues, fibro-glandular, muscles, and benign masses are visualised by the bright intensities where fat tissues become dark. There are two types of calcifications, such as micro and macro calcification. Whereas, the micro-calcification is the primary focus of the researchers because of its silent aggressiveness and detection complexity. It becomes visible as white regions in the mammography image when micro-calcium is deposited on the breast tissues, as shown in Fig. 1 (Shi et al., 2018).

However, the abnormal lesion such as micro-calcification region is the primary signal of breast cancer, which is the clear

Peer review under responsibility of King Saud University.

Production and hosting by Elsevier

E-mail address: s.hossain@ecu.edu.au

https://doi.org/10.1016/j.jksuci.2019.10.014
1319-1578/

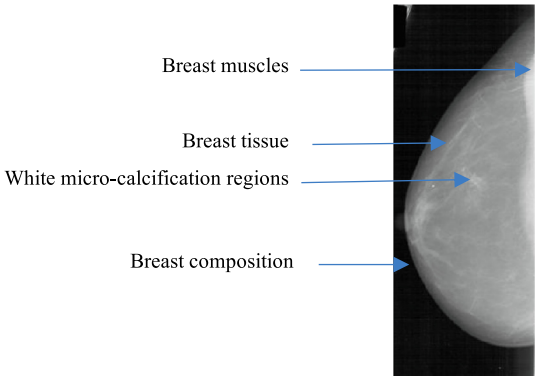

Fig. 1. Breast mammographic image.

indication of the cell death localised in that region. The segmentation of micro-calcification regions is complicated because of diversity, tinny, unclear visibility. The intensity difference between the normal breast tissue and micro-calcification regions is minimal for highly dense breast. The structure of micro-calcification is isolated or concentrated. Each region is a hetero-generous or irregular shape with 0.7 mm to 2 mm width (Marrocco et al., 2018). Therefore, deep observation is required for expert radiologist to detect the micro-calcification area.

However, the rapid growth of the patients increases the diagnostic process time to identify the suspicious regions by the limited number of experts while confusion is created on the diagnosis report. Sometimes active micro-calcification region is missed by the radiologist during the mammography image diagnosis (Alam et al., 2018; Bougioukos, 2010). According to the breast imaging report, the micro-calcification is defined within a range from 2 (benign) to 5 (malignancy) depending on their density, shape and the amount of region distributed in the breast tissue (Valvano et al., 2019). The principal motivation of the proposed work is to segment the micro-calcification regions ideally and can assist the radiologist in generating the diagnosis report correctly.

The paper presents as follows: section II, a brief description is given about previous works on micro-calcification segmentation where deep learning algorithms are used. In part III, the preprocessing of mammogram image is mentioned. Besides, the automatic feature extraction of micro-calcification and segmentation are explained. The Modified U-net deep learning neural network architecture is constructed and implemented to segment the micro-calcification regions. In part IV, the experimental results are reported, and other states of the art methods are performed according to the references to figure out the accuracy and comparison. The discussion is included in part V. Finally, the conclusion is presented in section VI, including the limitation and further extension of the proposed work.

2. Previous works

The medical imaging technologies integrated with deep learning algorithm which enhance the capability to segment the normal and abnormal breast tissues. Also, this integrated architecture improves the overall accuracy of the diagnosis. Whereas, quite a lot of deep learning methods are already proposed to segment lesion from the mammography images. Since our concern is to segment the micro-calcification in the breast regions. Therefore, we present some existing algorithms of micro-calcification segmentation. In general, all these approaches are divided into three parts: image preprocessing is applied to enhance the images; region of interest (ROI) is detected, and the regions of micro-calcification are separated from the other regions; deep learning based neural network is employed to train up the features, and the micro-calcification regions are classified.

(Chikamai et al., 2015) investigated a combined filtering method to identify calcification regions. Wavelet, Gaussian, median and finite impulse filters are collectively employed to improve the overall performance of this method. Though these filters provide better results individually, the artifacts are created along with the curve line. At the end of the process, the threshold method based on the entropy is applied to detect calcification regions from the background. Shin et al. (Shin et al., 2014) presented a technique based on discriminative restricted Boltzmann machine (DRBM). In this method, the micro-calcification regions are automatically learned by the morphology of calcified regions. The intensity points of the local peak are calculated to extract the patches from the mammogram images. The region which has no local intensity peak is considered as non-calcified regions. Afterwards, the training patches are manually annotated by the radiologist as the negative or positive patches. The micro-calcification regions exist in the positive patches. These positive samples are used to train the DRBM classifier. In the testing stage, the local peak intensity is extracted from the given image, and then DRBM is applied to classify the calcification regions.

(Lu et al., 2016) proposed a multi-stage cascade method. The poison distribution is used to remove the noise at the preprocessing stage in this approach. Then the individual candidate region is detected by the pixel-based classifier, which calculates the likelihood of the pixel. The shape and appearance features are applied to select the appropriate regions and eliminate the false positive regions. Whereas the area, circularity, regularity, and perimeter are considered as the shape and appearance features. Next, the clustering algorithm is performed on the individual micro-calcification region, and the connected components are estimated. Though less than three connection between the components is rejected. The morphological approach is presented by (Ciecholewski, 2017) where the image contrast is improved, and noises are removed in the preprocess section. After that, watershed segmentation is employed to classify the micro-calcification. However, the ROI regions are tested only in this method, which is taken from the mammogram images. Another automated segmentation approach of the micro-calcification cluster is developed by Alam et al. (Alam et al., 2018). In this approach, the region of interest are manually selected, and the wavelet-based process is applied to enhance the spatial image frequency in the preprocessing part. Then micro-calcium cluster is segmented using morphological operation and area ranking analysis. The image patch is split into small sub-regions. Then bi-cubic interpolation is applied on each sub-region to extract the background intensity level, and maximum 5% intensity level is selected to create the binary image. After that, the area ranking technique is employed to select the micro-calcification regions. Only the individual blob with 50% region of the pre-defined range is taken in this method. However, the detection of micro-calcification regions depends on the pre-defined range. Therefore, the regions which have a higher range than the pre-defined range are not detected. The median fuzzy C-means method is implemented by (Kowsalya and Priyaa, 2016) to detect the calcification regions. Generally, the fuzzy C-means and K-means clustering algorithm are calculated to find the mean and to determine the centroid. However, this method is not suitable for the segmentation of micro-calcification regions (Singh et al., 2012). Arikidis et al. (Arikidis et al., 2015) preferred a two-stage semi-automatic segmentation method to investigate the micro-calcification regions. The segmentation approach of level set is applied to detect the most significant ROI. Then the active contour model is employed to refine and to select the micro-calcification

regions. The selected regions are given into support vector machines (SVM) to learn and classify the micro-calcification regions (Gowrishankar et al., 2012).

Lakshmi et al. (2015) proposed an unsupervised segmentation method to classify the micro-calcification. The grayscale conversation, histogram equalisation and fuzzy contrast enhancement are applied to enhance the mammogram images. Then suspicious regions are detected by the particle swarm optimisation. The features which contain micro-calcification are separated from the other features based on the energy values. These values are estimated from the image wavelet transform. Finally, the micro-calcified regions are classified by the SVM. Shi et al. (2018) developed a hierarchical method together with image preprocessing and region segmentation to identify the calcification location. At first, the gradient magnitude is mapped in the mammogram images to detect the skin-air boundary. After that, the segmentation approach is applied for two times. One for the pixel-wise clustering where K-means clustering is used to segment the whole breast region and the second segmentation is employed to distinguish the breast regions from the pectoral muscle. Finally, the calcified regions are identified by the Law's texture filter. However, multiple segmentation increases the probability of information loss. The statistical approach of micro-calcification segmentation is adopted by Singh et al. (2017). Laplacian filter is used to enhance the image brightness at the preprocessing unit. The ROI is extracted across the whole image, where the size of each ROI is 32×32 pixels. The number of ROI is reduced by the image histogram, and the ROI which has micro-calcification regions are considered. The pixels in the normal regions are distributed. However, the pixels in the micro-calcification regions are concentrated and represented by the few bins of the image histogram. The skewness, kurtosis and entropy statistical feature are used to select the accurate ROI, which has micro-calcification regions. Finally, the four wavelet features are applied to distinguish normal and micro-calcified ROI. In this method, the total 648 ROI, which has micro-calcification and 1228 ROI without micro-calcification regions are extracted from the 25 images. All ROIs are taken to train the feedforward deep neural network (Abirami et al., 2016).

(Duraisamy and Emperumal, 2017) proposed a method where the Chan-Vese level segmentation technique is used to get the contour of the calcify region in the mammogram image. Then transformation and normalisation techniques are employed to prepare the segmented ROI. The preprocessed ROI is fed in the convolutional neural network (CNN) to learn the features. At the last step of the CNN, fully complex-valued relaxation network is employed to classify the calcified region. An intelligent system is investigated by Rehman et al. (2017). In this method, the adaptive threshold technique is applied as preprocessing to remove the noise from the mammogram images. Then canny edge detection technique is employed to detect individually micro and macro calcification regions. The micro-calcification region is carefully chosen based on the concentrated region by Otsu's algorithm. The features of micro-calcification regions are learned by CNN, and the classification is performed. However, the existing deep learning method is typically involved with loss to detect the micro-calcification regions. If the image size is large, then the regions of micro-calcification may be very small. When the image is resized to employ CNN, this small information is lost. Therefore, a lossless deep learning network for micro-calcification detection is implemented by Sulam et al. (2017). In this method, the whole image is decomposed into grid patches and screening network is employed to analyze each patch. Then VGG-m network where the first five layers are taken and the rest of the two fully connected layers with 512 filters are employed to finalize classification. Kaur et al. (2019) presented a method to detect the cancer region from the mammography images. In this method, images are pre-processed by the several techniques such as noise removal, filtering and morphological operations to identify the location of the ROI. After that deep learning algorithm such as CNN is used to train the ROI and multiclass SVM with K-means clustering is employed to classify the cancer regions. In this method, the unnecessary region is detected with the clustering algorithm, which decreases the efficiency of this method. Li et al. (2019) proposed a method where images are normalised by the zero-mean normalisation. Then images are enhanced by the random cropping and affine transformation to overcome the overfitting problem. Afterwards, DenseNet-II network model is used to train and classify the regions. However, each network layer is connected with the previous layer, and the features are reused from the previous layers. Therefore, the network is not strong enough to classify the calcified regions in the higher challenging images. According to Valvano et al. (2019), Otsu thresholding is applied to enhance the suspicious regions as a pre-processing of the images. Two CNN architecture is developed. First CNN is used to detect the micro-calcification regions from the square patches where the patches are manually extracted from the mammogram images. The positive label is assigned for each patch which has micro-calcification regions. The second CNN is used to segment the micro-calcification pixels. In this approach, manual patch extraction is required, which is time-consuming for the large data set (Trovini et al., 2018).

According to the above methods, the image preprocessing is employed to enhance the image intensity to get a better visualisation of the micro-calcification regions. After that, the ROI is identified based on the pixel intensity. Finally, the appropriate segmentation method is applied to classify the micro-calcification regions. In the proposed work, the image is enhanced with the Laplacian filter. Then the skin and air boundary are defined with gradient magnitude to separate the background from the image. Afterwards, the K-means clustering is applied to distinguish the pectoral region and breast region. Next, the automatic suspicious regions are detected with the frequency histogram technique where the optimum threshold value for frequency histogram is selected by the fuzzy C-means clustering. Then the suspicious regions are separated into positive and negative patches where the micro-calcification pixels exist in the positive patches. Finally, the modified U-net segmentation network is developed to train the positive patches. However, the proposed method provides higher performance among the recent deep learning methods and able to segment the micro-calcification regions efficiently at any size or appearance.

3. Proposed method

It is a challenging task to segment the micro-calcification regions because of the shape and size are very small and similar to the other non-calcification regions. However, the proposed method is contextually divided into five stages- the image preprocessing, the segmentation of breast regions, the extraction of suspicious patches, the selection of positive patches and train the segmentation network. The workflow is presented in Fig. 2.

3.1. Image enhancement

The contrast of the mammographic image is inferior. Therefore, it is complicated to examine ROI. It is required to sharp the suspicious regions to detect the salient features and classification in the next stage. While the micro-calcification pixels are brighter than the surrounding regions. Thus, the Laplacian filter provides better results, as shown in Fig. 3(b). The local Laplacian filter is first introduced by the Paris et al. (2015), and this filter can produce

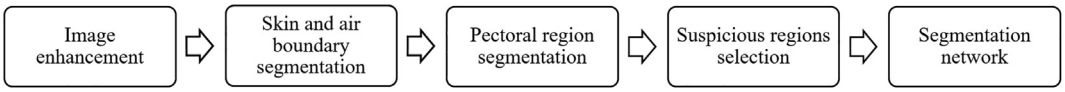

Fig. 2. Workflow of the micro-calcification segmentation using modified U-net segmentation network.

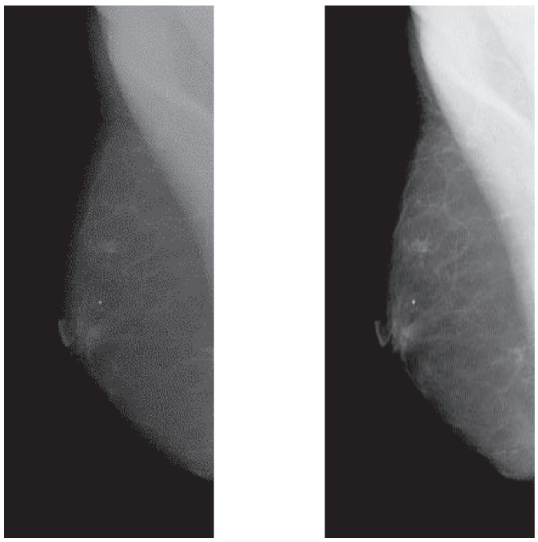

Fig. 3. The example of the mammogram image before enhancement (a); after enhancement with Laplacian filter (b).

high-quality output without any halos. However, the speed of this filter is quite slow. Therefore, the modulation operation is applied to enhance visual quality. If the input image is $V = \{v(m,n)|1 \le m \le H, 1 \le n \le W\}$ where the size is $H \times W$. The set of luminance is $[v_l, v_u]$ where $v(m,n) \in [v_l, v_u]$. The luminance mapping (LM) computes every luminance level and restrains the luminance level using the mapping, which has a large difference between the luminance level. Therefore, the image enhancement at the luminance O_{LM} within the range $[o_l o_u]$, where, $O_{LM} = \{o(m,n)|1 \le m \le H, 1 \le n \le W\}$ and $o(m,n) \in [o_l v_u]$; $[o_u v_u]$. If $V = \{v_1, v_2, \cdots\cdots, v_N\}$ and $O = \{o_1, o_{2,\cdots\cdots}, o_N\}$ is the set of stored N distinct luminance then the output image would be O_{LM}. Where, $v_1 = v_l < v_2 < \cdots < v_N = v_u$ and $o_1 = o_l < o_2 < \cdots < o_N = o_u$. The mapping of the luminance level is as follow:

$$o_i = \varphi(v_i) = v_i + \omega f(i) \tag{1}$$

where, ω is the modulation parameter of the luminance and $i = 1, 2, \cdots N$. The Eq. (1) transforms the luminance of the image V into the enhanced luminance of the output image O_{LM}. The $f(i)$ is explained as follow:

$$f(i) = \sum_{j-1}^{i-1} \left(g_j^{'} - g_j\right) \text{ when } i > 1; \text{otherwise } f(i) = 0 \tag{2}$$

where, $g_j^{'} \in G_{o_{LM}}; G_{o_{LM}} = \{g_1^{'}, g_2^{'}, \ldots g_{N-1}^{'}\}$ and $g_j \in G_v; G_v = \{g_1, g_2, \ldots g_{N-1}\}$. The $G_{o_{LM}}$ and G_v are the set of stored luminance difference. The regenerated difference is as follows:

$$g_j = v_{j+1} - v_j \tag{3}$$

$$g_j^{'} = k + [g_j - k]^{S[g_j - k]} \tag{4}$$

where, $S(x) = 0$ when $sgn(x) = 1$ otherwise, $(x) = \alpha$; $k = min\{G_v\} + (max\{G_v\} - min\{G_v\}).\beta$; α and β are defined as the control parameters of the luminance. The micro-calcification regions emerge with enhanced value, and the value of the surrounding pixels gets suppressed (Bhupendra Singh et al., 2017).

3.2. Skin and air boundary segmentation

The skin and air boundary segmentation are, as shown in Fig. 4. The weight of each pixel is calculated based on gradient magnitude. The 3×3 cross window is applied for each pixel, and the array of weight is created (W). The weight is inversely connected with the gradient magnitudes on the horizontal and vertical direction. Therefore, the high-intensity regions are split from the low-intensity regions because of the gradient magnitude changes profoundly at the edge regions. Then, the horizontal line fitting approach is applied to get rid of artifacts such as labels, scratches and markers etc. The minor gradient noises are eliminated by the image erode method (Zhang et al., 2014). The thin lines are erased where the highest body of the gradient weights are preserved. Thus, the largest part of the breast and pectoral regions are retained, as shown in Fig. 4(a). The connected pixel area approach is applied to remove the small artifacts. The connected pixel components are labelled, and the areas are calculated. Each area is compared with the suitable pre-set value where pre-set value is smaller than the micro-calcification areas.

3.3. Pectoral region segmentation

The K-means pixel-wise clustering is used to distinguish different tissues structure such as breast and pectoral tissues where the strong pixel difference exists between the nearest pixels. The city block distance metric is applied to calculate the distance between the nearest pixels. If the intensity of the image pixel $P(x,y)$ is represented by $(I_{(x,y)})$and gradient weight is $(W_{(x,y)})$ then the clustering equation is as follow:

$$d_{cityblock}(p_1 p_2) = \sum_{j=1}^{n} |p_{1j} - p_{2j}| = |I_1 - I_2| + |W_1 - W_2| \tag{5}$$

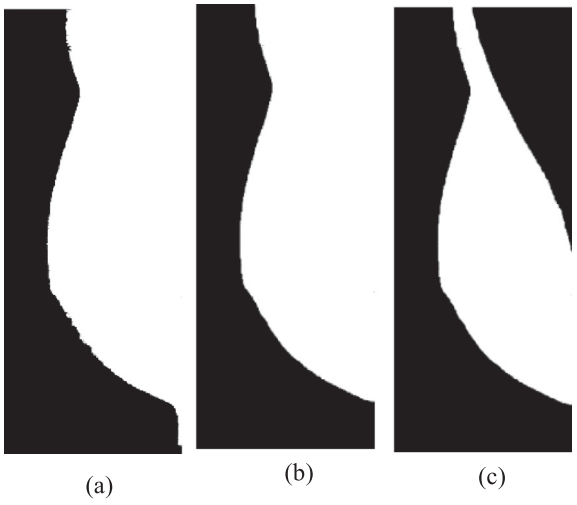

Fig. 4. The example of skin and air boundary segmentation (a); the breast region after noise removal (b); pectoral region segmentation (c).

Here, P_1 and P_2 are the two pixels within the same regions and P_{ij} defines the feature of j-th position. The pixels are labelled into two classes by the unsupervised clustering in the feature space. The breast tissues combining with pectoral tissues are separated. Then pectoral tissues are pulled out according to the similar gradient weights and the intensities of the pixels in the cluster, as shown in Fig. 4(c).

The morphological operations are employed to find the accurate boundary between the breast and pectoral tissues. In this work, Matlab built-in functions are applied for smooth out the edges of the boundary. The regions of the segmented cluster are adjusted by removing the too-small areas where the threshold of the area is 100 pixels. The erosion and dilation are performed, which is 3×3 pixels in wide. The gaps and holes are filled where the connectivity of four neighbouring pixels exist. Finally, the segmented breast regions are extracted (Pan, 2017).

3.4. Suspicious regions selection

The example of the mammogram image and the cross-section of the suspicious patch are as shown in Fig. 5. The detection of the suspicious regions is as shown in Fig. 6. The high pass filter is applied to enhance the contrast of the suspicious regions, as shown in Fig. 6(a). Initially, the image is divided into equal size of contextual regions and the histogram is calculated for each region. The clip limit of the threshold is introduced where the high clip limit enhances the intensity of the suspicious regions. The histogram of the contextual regions is redistributed in a way that it does cross the clip limit. This technique finds the high-intensity objects. After that, the morphological opening is applied to create a grayscale image correspond to the region of breast tissues, as shown in Fig. 6(b). Therefore, the background regions are obtained and subtracted from the mammogram image. This process is used to visualise the bright spot on the darker background regions, as shown in Fig. 6(c) (Bougioukos, 2010; Dholey, 2018). The frequency histogram technique of the connected pixels is used to detect suspicious regions. The fuzzy C-means clustering method is utilised to determine the optimal threshold for the frequency histogram method. The frequency histogram technique is related to the morphological operation of the neighbouring pixels. If the pixel $I(i,j)$ where the image dimension is $N \times M$ then the neighboring pixel $D(i,j)$ of the given pixel $I(i,j)$ is as follow:

$$D(i,j) = \{\varphi_{i,j} \subset \{I(i,j)\}_{N\times M}\} \tag{6}$$

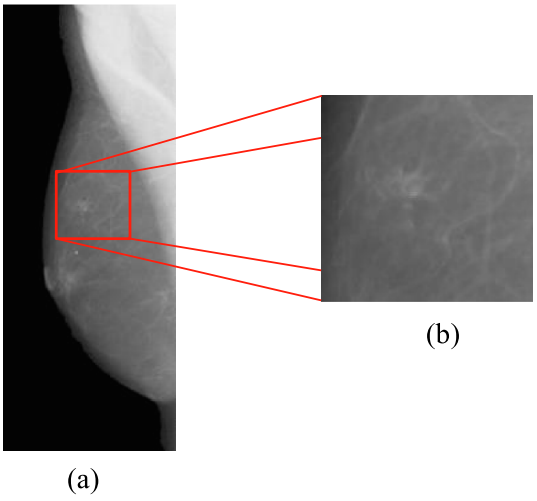

Fig. 5. The example of the mammogram image (a); the cross-section of the suspicious patch (b).

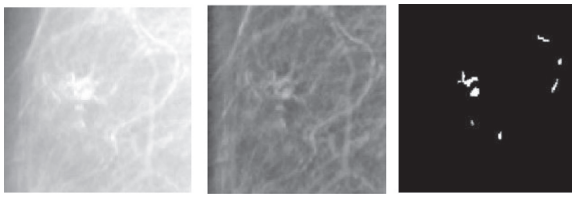

Fig. 6. The example of the cross-section after high pass filter (a); the morphological opening is applied (b); frequency histogram for connected pixels (c).

where the user-defined scanning is represented by $\varphi(i,j)$. The scanning process is done by slicing the image into non-overlapping windows. The reason for selecting the non-overlapping window is to reduce the computational complexity. The size of the window depends on the morphological component. Usually, the suspicious regions are the small connected bright pixels inside the breast regions and separated from the surrounding high-density tissue, as shown in Fig. 6(b). The (3×3) window size is enough to cover the neighbouring area of the certain pixel (i,j) and the pixel intensities are multiplied with the filter weights. However, the final segmented output depends on the morphological masking operation to determine the connected pixels. The size of the mask is (3×3) where the border pixels of one pixel wide is considered as less important. The connected neighbouring pixels are defined as $[T-c, T+c]$, where, the grayscale intensity range is defined by the integer value c, and T is the known greyscale value. At each window scanning, the parameter c is computed within the range. Therefore, the parameter c has no global value for the mammogram image. Whereas the value of c depends on the value of neighbouring pixels at each scan. Then the number of connected pixels is measured by the frequency histogram. The optimum results are obtained when the pixel distribution is well apart corresponding to the two peaks: background and suspicious regions. The final segmentation output is found by the threshold value, which is within these two peaks. The threshold value is calculated with the fuzzy C-means algorithm, which is designed to get the two cluster of the connected pixels. The connected pixels of micro-calcification and non-micro calcification regions are extracted by the first cluster, whereas the second cluster is used to cluster the surrounding background. The optimal threshold is used to intersect the two cluster on the grayscale axis. The iterative approach of clustering algorithm finds the centroid of the cluster and minimises the dissimilarity as follows:

$$J(U, c_1, c_2, \cdots, c_c) = \sum_{i=1}^{c} J_i = \sum_{i=1}^{c} \sum_{j=1}^{n} u_{ij}^{m} d_{ij}^{2} \tag{7}$$

where the c_i defines the centroid of the cluster i. The $d_{i,j}$ defines the Euclidian distance between the centroid and the data point j. The $u_{i,j}$ defines the fuzzy function matrix of $U = u_{i,j}$ where $0 \leq u_{i,j} \leq 1$. The m represents the weighting exponent and experimentally determined the optimal value is $m = 2$. During the iteration, the cluster centre is modified by the algorithm, and the neighbouring data member is changed until to minimise the dissimilarity function (Bougioukos, 2010; Jemimma and Raj, 2018; Wisaeng and Sa-Ngiamvibool, 2018).

3.5. Segmentation network

The manual observation is required to assign the positive and negative mark for the bounding box after automatically identify the suspicious regions, as shown in Fig. 7(a). The positive bounding boxes contain the micro-calcification pixels, as shown in Fig. 7(b).

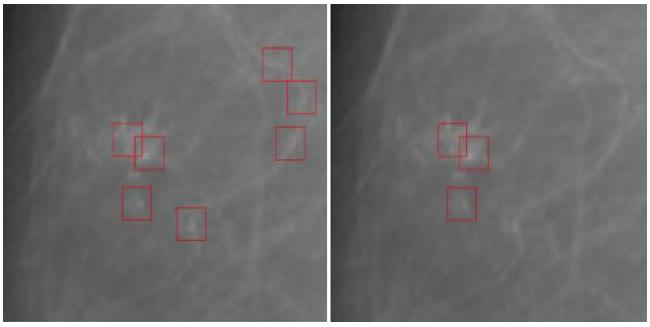

Fig. 7. The example of suspicious regions (a); the regions contain micro-calcification pixels (b).

All the positive boxes are fed into the segmentation network to train the network for classification. The proposed segmentation network is modified and developed based on the conventional U-net segmentation network, as shown in Fig. 8. The modification of the proposed network is to focus on automatic training models. The U-net is a combination of the encoder and decoder network. The encoder part is the traditional CNN, which contains semantic information and less spatial information. However, spatial information is also essential with semantic information for the segmentation. The U-net gets the particular information from the decoder part where semantic information is collected from the lowermost layer of the U-net network. The high-resolution features are combined in the decoder part, which is directly obtained from the encoder part by skipping connection and provides the fine segment structures. In this work, the segmentation network is designed by the two convolutional layers. These two layers are added between the pooling layers at the encoder part, and the convolutional operations are transposed at the decoder part. The rectified linear unit (ReLU) is changed by the leaky ReLU, and instance normalisation is applied instead of batch normalisation (Ulyanov et al., 2016; Ioffe and Szegedy, 2015). The patch size is 32 × 32 pixels, and the batch size is 42 feature maps for the highest layer. The four pooling operations are set to train the entire slice effectively. Assume, the input is x_l in lth layer and (i,j) is the centre pixel of each patch on kth feature. The output of the network $O^l_{ijk}(t)$ for t time step is as follow (Zhou et al., 2018; Isensee, 2018; Askari Hemmat et al., 2019):

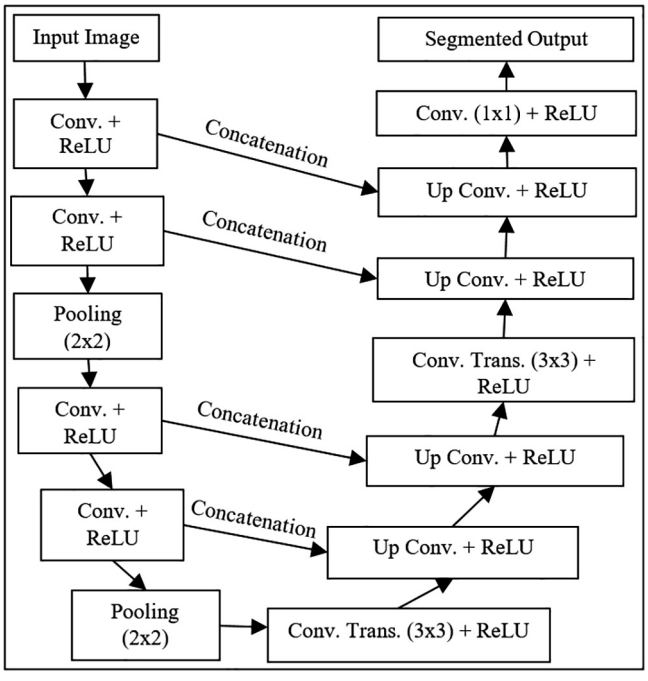

Fig. 8. The architecture of the modified U-net segmentation network.

$$O^l_{ijk}(t) = (w^f_k)^T x^{f(i,j)}_l(t) + (w^r_k)^T x^{r(i,j)}_l(t-1) + b_k \tag{8}$$

where the inputs of the convolutional layers are $x^{f(i,j)}_l(t)$ and $x^{r(i,j)}_l(t-1)$. The weight of the convolutional layers are $(w^f_k)^T$ and $(w^r_k)^T$. The bias is b_k. The output is fed into the Leaky ReLU, and the activation function (f) is as follow:

$$\mathcal{F}(x_l w_l) = f\left[O^l_{ijk}(t)\right] = \max[0, O^l_{ijk}(t)] \tag{9}$$

where $\mathcal{F}(x_l w_l)$ is the output of CNN unit. This output is used for down-sample and up-sample at the encoding and decoding part. The forward CNN part is, as shown in Fig. 8. The features are collected from the encoding part to the decoding part in this CNN based segmentation network. However, the features are collected inside the model, which improves the learning and testing stages, unlike the conventional U-net model. This approach provides a robust feature representation. It is very effective for extracting the low-level features which is essential for the micro-calcification segmentation. The concatenation operation is used instead of using cropping and copying, which are applied in the basic U-net model. A large number of parameters have a significant impact on the training and testing efficiency. The limited number of the parameters are employed in this network, which provides higher accuracy. All the changes in the U-net model provide better micro-calcification segmentation result, which is outperformed among the current methods.

The significances of this study are as follow: The proposed segmentation network is applied on the Digital Database for Screening Mammography (DDSM) images to segment the micro-calcification regions; The quantitative evaluation is done with sensitivity, precision, accuracy, F-measurement, Jaccard index and Dice score. The recent existing methods are implemented, and the comparison is conducted.

4. Experiment and results

The modified U-net segmentation network is built and positive patches are trained by the MAT-LAB platform (The MathWorks Inc, Natick, USA) where the deep learning toolbox is used combining with the image processing toolbox. The GeForce RTX 2080 Ti graphics processing unit and core i7 processor is utilized in this work.

4.1. Digital database of mammography screening

The mammogram images are collected from the University of South Florida Digital Mammography website. The Digital Database for Screening Mammography (DDSM) is available for the research analysis (Samala et al., 2018). 2620 case studies are comprised in this database by craniocaudal and mediolateral oblique breast view. In each study, there are two images of each breast, including the information of the patients such as age, information about the breast density and abnormalities. The data sets are divided based on the image acquisition scanner, spatial resolution and different sorts of suspicious areas. Each file is a portable grey map format. In the database, similar cases are stored in each volume. The normal cases are created with the previous screening exam and the next screening exam after four years later. The cancer cases are consisted of at least one pathologist found the cancer region. The

Benign instances are made up of any suspicious is located in the breast regions. There are 01 to 15 cancer volumes existed and contained 914 cases taken by LUMISYS, DBA and HOWTEK scanners with 12-bit depth including ground truth regions. For this work, the mediolateral oblique view image of each patient is taken.

4.2. Data augmentation

The overfitting problem occurs when a deep network is trained with a limited number of patches. The patch augmentation makes accurate sense in the segmentation of micro-calcification because of the irregular shape, appearance and different orientation of the micro-calcification. The variety of data augmentation techniques are applied during the training time to increase the number of positive patches. So that the network can learn from the different transformations of patches as well. The simple alterations of patches are applied. The scaling and translation methods are used to create more synthetic and artificial patches. The patches are flipped horizontally and perpendicularly. Afterwards, the $90^{\circ}, 180^{\circ}$ and 270° degree rotations are implemented on the patches. The augmentation approaches are only applied to the set of positive training patches, which improves the training as well as the segmentation accuracy.

4.3. Training procedure

The positive patches are divided into three groups, where 60% is for training, 20% is for validation, and 20% is for testing. The dimension of the patch is set 32×32 pixels experimentally concerning the computational burden of the modified U-net segmentation network. However, manual observation is required to mark the positive and negative patches after the automatic selection of suspicious and non-suspicious regions. However, the pixels of micro-calcification exist in the positive patches. The 3×3 kernel is used in the convolutional layer. The 2×2 kernel is applied in the pooling layer followed by a convolutional layer. In the decoder part, the convolutional transpose is employed, followed by the concatenation layer. The concatenation is applied between the encoder and decoder part in this method, which provides features map as output. This features map is developed by an activation function with the 1×1 convolutional layer. After that, the segmented area is generated based on the threshold value (T), which is experimentally set as 0.5 in the proposed approach. The segmentation model is assessed with five-fold cross-validation. The test patches are divided into five groups, and the average accuracy is collected, as shown in Table 1. The network is trained with a combination of cross-entropy and dice loss (similarity matric) as follows (Isensee, 2018):

$$L_{Total} = L_{Dice} + L_{CE} \tag{10}$$

The dice loss is computed for every sample in each batch and implemented as follows:

$$L_{dc} = -\frac{2}{|K|}\sum_{k\in K}\frac{\sum_{i\in I} u_i^k v_i^k}{\sum_{i\in I} u_i^k + \sum_{i\in I} v_i^k} \tag{11}$$

where u and v are the output of the softmax and define as the ground truth. The $I \times K$ is the shape of u, and v individually where $i \in I$ is the number of pixels in each training patch and $k \in K$ is the number of classes. The batch size of the training is 42 for each epoch. The average of exponential moving is set to train the loss and validation. The initial learning rate is 3×10^{-4}, and the rate is decreased by the factor 5 after 30 epochs to increase the minimum learning rate about 5×10^{-3}. The learning session is terminated when the rate is 5×10^{-3} within the 60 epochs. However, the learning loss depends on the number of iterations, and the loss is decreased when the number of iterations is increased. Whereas, the 15% accuracy depends on the mini-batch size. A large number of inputs and weights at the final layer indicates the minor information loss and great capability of learning. The region of ground truth and the segmented region with the proposed method, as shown in Fig. 9.

4.4. Quantitative evaluation

The information of the ground truth for each mammogram image exists in the DDSM data set, which provides an extra advance for quantitative evaluation. The several evaluation criteria such as sensitivity, precision, accuracy and F-measurement are calculated as follows (Li et al., 2019; Pan, 2017):

$$Sensitivity = \frac{TP}{TP + FN} \times 100 \tag{12}$$

$$Precision = \frac{TP}{TP + FP} \times 100 \tag{13}$$

$$Accuracy = \frac{TP + TN}{TP + TN + FP + FN} \times 100 \tag{14}$$

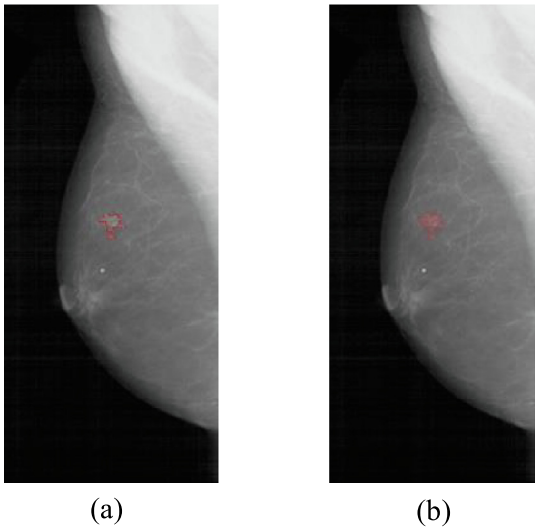

Fig. 9. The mammogram image with ground truth (a); the segmented region of the micro-calcification with the proposed method (b).

Table 1
Performance of the proposed method.

Set	Sensitivity	Precision	Accuracy	F-measure	Dice Score	Jaccard Index
1	98.7%	95.2%	98.5%	98.8%	98.1%	97.7%
2	98.4%	94.4%	98.2%	98.5%	97.8%	97.2%
3	98.8%	94.7%	98.6%	98.9%	98.3%	97.8%
4	97.6%	93.8%	97.4%	97.7%	97.2%	96.7%
5	98.5%	95.7%	98.3%	98.6%	97.9%	97.3%
Mean	98.4%	94.7%	98.2%	98.5%	97.8%	97.4%

$$F-measure = \frac{2 \times Recall \times Precision}{Recall + Precision} \times 100 \quad (15)$$

where the TP defines the true positive, which can accurately segment the micro-calcification region. The TN states for the true negative, which segments the area leaving the valuable part of the micro-calcification regions. The FP equals the false positive, which segments the region falsely as micro-calcification. The FN stands for the false-negative, which segments the micro-calcification with unnecessary regions. Here, recall is considered as sensitivity. The diversity and similarity between the ground truth and the region of segmented micro-calcification are measured with the Jaccard index. While the Dice score only represents the similarity matrix between the ground truth and the region of segmented micro-calcification. The equations are given as follow:

$$Jaccard\ Index = \frac{TP}{TP + FN + FP} \quad (16)$$

$$Dice\ Score = \frac{2.TP}{2.TP + FN + FP} \quad (17)$$

The positive patches are divided into 5 sets to improve the training efficiency and reduce the training complexity, as shown in Table 1. The dimension of the patch is 32×32 pixels, which provides better output. According to the statistical data on Table 1, the sensitivity is relatively constant for the patch set 1, 2 and 3, but the overall sensitivity is 98.4% whereas precision is 94.7%. However, the accuracy is dropped for the patch set 4, but the mean accuracy is 98.2%, which is quite satisfactory. The average Dice score is 97.8%, which is the similarity pixel matrices between ground truth and the segmented region of the micro-calcification with the proposed method. The average Jaccard index is 97.4%. The final accuracy of the modified U-net segmentation network is 98.2% for the test patches. The false-positive ratio (FPR) is very high for most of the classical approaches to detect the micro-calcification regions. In the proposed method, the FPR is calculated and obtained0.003%.

4.5. Comparison with existing methods

The performance of the proposed method is compared with the recent existing methods. The existing deep learning methods are implemented according to the references and comparison are executed with the same DDSM data set. The accuracy of the recent methods is presented in Table 2. All the state-of-the-art methods are validated with the same procedures. The accuracy of the CNN method provides better performance, about 97.4% among the other standing methods. In this method, two CNN models are developed where the first one is used as a detector to detect the region of interest, and the second one is applied for segmentation to classify the micro-calcification regions. However, the same network architecture is shared by both CNN models, which reduces the network burden. According to the reference, the network architecture is developed with 6 convolutional neural layers where the kernel size is 3×3. The stride is 1, including 2 fully connected network layers containing 64 units. The patch size is gradually reduced from 32×32 to 2×2 features which provide as input in the fully connected layer. However, the network can not extract the features from the whole patches, and there is no proper strategy to maintain the overfitting. The deep network provides the gradient dispersion where the gradient is disappeared in the network for backwards propagation. All the difficulties are considered in the proposed method. Therefore, the performance of the proposed method is 98.2%, which is higher than the CNN method. The accuracy of the Decision Model Deep Learning method is intermediate about 95.6%, which is built with the convolutional layers, pooling layers, max-pooling layers and fully connected layers. However, the ReLU layer is used as an activation function in the convolutional layer to increase the attributes of the nonlinear decision, which affects the upper stated layer. Therefore, the precision of localisation is decreased. The performance of the DenseNet-II Neural Network is slightly poor, approximately 94.5% because of the network layers. The DensNet layer becomes wider according to the iterations. Though the deeper and wider network able to provide better training accuracy but it increases the number of parameters, computational memory as well as the overfitting problem. Therefore, the network trains loosely. According to the reference, the 40 network layer is assigned, and the growth rate is 12, including the 3 DenseNet block layers where the transition layer is 3. Therefore, it is difficult to find the optimal setting of the parameter for DenseNet network.

Table 2
Comparison with existing methods.

Methods	Number of Parameters (in millions)	Accuracy
Decision Model Deep Learning Method (Rehman et al., 2017)	2.61	95.6 %
DenseNet-II Neural Network Method (Li et al., 2019)	3.03	94.5 %
Convolutional Neural Network Method (Valvano et al., 2019)	2.80	97.4 %
Proposed Modified U-net Method	0.84	98.2 %

5. Discussion

The proposed method is executed, which provide better performance in every step than the existing methods. However, the accuracy of the proposed method depends on the efficient segmentation of air-skin boundary and the accurate segmentation of pectoral regions. The proposed method provides the highest performance around 98.96% for the segmentation of the air-skin boundary with the pectoral tissues. Afterwards, the segmentation accuracy of the pectoral regions is about 98.87%. However, (Czaplicka and Włodarczyk, 2011) proposed a method for air-skin boundary separation where accuracy is roughly 98.11%, and the segmentation of the pectoral region is almost 98.05%. The segmentation of the breast-pectoral regions without considering the air-skin boundary line are focused by some researchers where the Maitra et al. (2012) achieved almost 95.7% accuracy by applying the region growing approach. The slightly higher accuracy of the air-skin boundary and pectoral region segmentation provide overall better segmentation output of the proposed method. However, the proposed method provides higher performance with the less number of parameters, which is the significant advantage regarding the processing time and the memory, as shown in Table 2. Therefore, the proposed method is outperformed than the existing methods. Also, it provides the foundation of further research focusing only on the segmentation of breast micro-calcification regions.

6. Conclusion and future work

The main objective of this work is to segment the micro-calcification regions efficiently with modified U-net segmentation network. The proposed method is quantitatively evaluated with the amount of overlap areas, which provides very similar results. The limitation of this work is to involve the expert radiologist for the qualitative analysis in the mammogram images. The manual observation by a radiologist which will increase the efficiency of the proposed method. The proposed method is developed based on the DDSM data set. However, the performance of this method

is very poor for the MIAS dataset. In this dataset, the intensity difference between the micro-calcification regions and the surrounding regions of micro-calcification are very small inside the breast region. It should be mentioned that the DDSM data set is the oldest mammographic database. It should be worthy of the proposed method is to apply on the mammographic data set of the new generation. In future, the proposed method would be adjusted to address this limitation. However, researchers are interested in using this DDSM data set because of containing a large number of mammographic images (Samala et al., 2018).

The early diagnosis of micro-calcification regions is crucial to prevent breast cancer. In this work, the automatic segmentation method of micro-calcification regions is proposed by developing a modified U-net segmentation network. Data preprocessing and the procedure to separate the breast region from the pectoral region are described elaborately. Then the positive patches are extracted which contain the regions of micro-calcification from the breast region. The several augmentation techniques are performed on the positive patches to avoid the overfitting problem. Afterwards, the obtained positive patches are fed into the proposed modified U-net segmentation network. The five-fold cross-validation is performed on the five sets of test patches. The proposed method decreases the segmentation of uncertain regions. It reduces the diagnosis time of the mammogram image, which is essential for the treatment of the breast calcification. Also, it can assist the radiologists effectively. In future, the proposed work can be implemented in the real-time mammography systems integrating the appropriate hardware and software interface for screening and diagnosis of the micro-calcification. On the other hand, the proposed approach would be improved by investigating other efficient and potential deep learning segmentation network.

References

P. Kaur, G. Singh, P. Kaur, 2019. Intellectual detection and validation of automated mammogram breast cancer images by multi-class SVM using deep learning classification, Informatics in Medicine Unlocked, p. 100151.

Shi, P., Zhong, J., Rampun, A., Wang, H., 2018. A hierarchical pipeline for breast boundary segmentation and calcification detection in mammograms. Comput. Biol. Med. 96, 178–188.

Pardamean, B., Cenggoro, T.W., Rahutomo, R., Budiarto, A., Karuppiah, E.K., 2018. Transfer Learning from Chest X-Ray Pre-trained Convolutional Neural Network for Learning Mammogram Data. Procedia Comput. Sci. 135, 400–407.

Li, H., Zhuang, S., Li, D.-A., Zhao, J., Ma, Y., 2019. Benign and malignant classification of mammogram images based on deep learning. Biomed. Signal Process. Control 51, 347–354.

C. Marrocco, et al., 2018. Mammogram denoising to improve the calcification detection performance of convolutional nets, In: 14th International Workshop on Breast Imaging (IWBI 2018), 2018, vol. 10718: International Society for Optics and Photonics, p. 107180W.

Alam, N., Oliver, A., Denton, E.R., Zwiggelaar, R., 2018. Automatic segmentation of microcalcification clusters. In: Annual Conference on Medical Image Understanding and Analysis, 2018. Springer, pp. 251–261.

Bougioukos, P. et al., 2010. Fuzzy c-means-driven fhce contextual segmentation method for mammographic microcalcification detection. The Imaging Sci. J. 58 (3), 146–154.

Valvano, G. et al., 2019. Convolutional Neural Networks for the segmentation of microcalcification in Mammography Imaging. J. Healthcare Eng. 2019.

K. Chikamai, S. Viriri, J.-R. Tapamo, The effectiveness of combining the likelihood maps of different filters in improving detection of calcification objects. In: 2015 Pattern Recognition Association of South Africa and Robotics and Mechatronics International Conference (PRASA-RobMech), 2015: IEEE, pp. 30-36.

S. Shin, S. Lee, I. D. Yun, 2014. Classification based micro-calcification detection using discriminative restricted Boltzmann machine in digitized mammograms. In: Medical Imaging 2014: Computer-Aided Diagnosis, 2014, vol. 9035: International Society for Optics and Photonics, p. 90351L.

Ciecholewski, M., 2017. Microcalcification segmentation from mammograms: a morphological approach. J. Digit. Imaging 30 (2), 172–184.

Kowsalya, S., Priyaa, D.S., 2016. An integrated approach for detection of masses and macro calcification in mammogram images using dexterous variant median fuzzy c-means algorithm. In: 2016 10th International Conference on Intelligent Systems and Control (ISCO), pp. 1–6.

Singh, N., Mohapatra, A.G., Rath, B.N., Kanungo, G.K., 2012. GUI Based Automatic Breast Cancer Mass and Calcification Detection in Mammogram Images usingK-means and Fuzzy C-means Methods. Int. J. Mach. Learn. Comput. 2 (1), 7.

Arikidis, N., Vassiou, K., Kazantzi, A., Skiadopoulos, S., Karahaliou, A., Costaridou, L., 2015. A two-stage method for microcalcification cluster segmentation in mammography by deformable models. Med. Phys. 42 (10), 5848–5861.

Gowrishankar, C., Balakumaran, T., Shanmugam, A., 2012. Active contour based micro-calcification detection and classification in digital mammogram. Aust. J. Electr. Electron. Eng. 9 (4), 367–376.

Lakshmi, S.V., Janet, J., 2015. Unsupervised segmentation based classification of microcalcification using SVM. Adv. Nat. Appl. Sci. 9 (7), 92–100.

M. Dholey et al., 2018. A Computer Vision Approach for Lung Cancer Classification Using FNAC-Based Cytological Images. In: Proceedings of 2nd International Conference on Computer Vision & Image Processing, 2018: Springer, pp. 181-195.

Z. Lu, G. Carneiro, N. Dhungel, A. P. Bradley, 2016. Automated detection of individual micro-calcifications from mammograms using a multi-stage cascade approach, arXiv preprint arXiv:1610.02251, 2016.

A. V. Bhupendra Singh, R. C. Tripathi, 2017. Contrast enhancement and micro-calcification detection using statistical and wavelet features in digital mammograms. In: Fourth International Conference on Image Information Processing (ICIIP), pp. 1-4. http://dx.doi.org/10.1109/ICIIP.2017.8313755.

Abirami, C., Harikumar, R., Chakravarthy, S.S., 2016. Performance analysis and detection of micro calcification in digital mammograms using wavelet features. In: 2016 International Conference on Wireless Communications, Signal Processing and Networking (WiSPNET), pp. 2327–2331.

Duraisamy, S., Emperumal, S., 2017. Computer-aided mammogram diagnosis system using deep learning convolutional fully complex-valued relaxation neural network classifier. IET Comput. Vision 11 (8), 656–662.

Rehman, M.A., Ahmed, J., Waqas, A., Sawand, A., 2017. Intelligent system for detection of microcalcification in breast cancer. Int. J. Adv. Comput. Sci. Appl. 8 (7), 382–387.

J. Sulam, R. Ben-Ari, P. Kisilev, 2017. Maximizing AUC with Deep Learning for Classification of Imbalanced Mammogram Datasets. In: VCBM, 2017, pp. 131-135.

G. Trovini et al., 2018. A deep learning framework for micro-calcification detection in 2D mammography and C-view. In: 14th International Workshop on Breast Imaging (IWBI 2018), 2018, vol. 10718: International Society for Optics and Photonics, p. 1071811.

Paris, S., Hasinoff, S.W., Kautz, J., 2015. Local Laplacian filters: edge-aware image processing with a Laplacian pyramid. Commun. ACM 58 (3), 81–91.

Pan, X. et al., 2017. Accurate segmentation of nuclei in pathological images via sparse reconstruction and deep convolutional networks. Neurocomputing 229, 88–99.

D. Ulyanov, A. Vedaldi, V. Lempitsky, 2016. Instance normalization: the missing ingredient for fast stylization, arXiv preprint arXiv:1607.08022, 2016.

X. Zhang, Y. H. Guo, G. Li, J. L. He, 2014. Vein Image Segmentation Based On One-Dimentional Gray And Filter Erosion Method. In: Appl. Mech. Mater. 2014, vol. 635: Trans Tech Publ, pp. 1049-1055.

Jemimma, T., Raj, Y.J.V., 2018. Brain Tumor Segmentation and Classification Using Deep Belief Network. In: 2018 Second International Conference on Intelligent Computing and Control Systems (ICICCS), pp. 1390–1394.

Wisaeng, K., Sa-Ngiamvibool, W., 2018. Improved fuzzy C-means clustering in the process of exudates detection using mathematical morphology. Soft. Comput. 22 (8), 2753–2764.

F. Isensee et al., 2018. nnu-net: Self-adapting framework for u-net-based medical image segmentation, arXiv preprint arXiv:1809.10486, 2018.

S. Ioffe, C. Szegedy, 2015. Batch normalization: accelerating deep network training by reducing internal covariate shift, arXiv preprint arXiv:1502.03167, 2015.

M. H. Askari Hemmat, S. Honari, Y. Savaria, J.-P. David, 2019. Quantization of U-Net Model for Medical Image Segmentation, 2019.

Zhou, Z., Siddiquee, M.M.R., Tajbakhsh, N., Liang, J., 2018. Unet++: a nested u-net architecture for medical image segmentation. In: Deep Learning in Medical Image Analysis and Multimodal Learning for Clinical Decision Support. Springer, pp. 3–11.

Samala, R.K., Chan, H.-P., Hadjiiski, L., Helvie, M.A., Richter, C.D., Cha, K.H., 2018. Breast cancer diagnosis in digital breast tomosynthesis: effects of training sample size on multi-stage transfer learning using deep neural nets. IEEE Trans. Med. Imaging 38 (3), 686–696.

Czaplicka, K., Włodarczyk, J., 2011. Automatic breast-line and pectoral muscle segmentation. Schedae Informaticae 20.

Maitra, I.K., Nag, S., Bandyopadhyay, S.K., 2012. Technique for preprocessing of digital mammogram. Comput. Methods Programs Biomed. 107 (2), 175–188.